Bulletin de la Société Royale des Sciences de Liège, Vol. 84, 2015, p 42 - 52

Photoprocessing of astrophysical ice analogs using the Interstellar Astrochemistry Chamber

Gustavo A. Cruz-Díaz[1,*], Rafael Martín-Doménech[2], Guillermo M. Muñoz Caro[2]

[1] Leiden Obseravtory (Universiteit Leiden), Niels Bohrweg 2,
NL-2300 CA, Leiden, The Netherlands
[2] Centro de Astrobiología (INTA-CSIC), Ctra. de Ajalvir, km 4,
Torrejón de Ardoz, 28850 Madrid, Spain

Abstract: UV-photodesorption is a plausible non-thermal desorption process in dark clouds, which is required to explain the presence of molecules in the gas phase. Models of ice photoprocessing depend on the vacuum ultraviolet (VUV) absorption cross section of the ice. In the past, gas phase cross section values were used as an approximation due to the lack of reported VUV-absorption cross sections of most molecules present in interstellar ice mantles (with the exception of H_2O, CO_2, and NH_3). ISAC is an ultra-high-vacuum (UHV) set-up where pure ices composed of H_2O, CO, CO_2, CH_3OH, NH_3, CH_4, H_2S, N_2, and O_2 were deposited at 8 K. The column density of the ice samples was measured *in situ* by infrared spectroscopy in transmittance. VUV-absorption spectra of the ice samples were collected in the 120-160 nm (10.33-7.74 eV) range using a commercial microwave-discharged hydrogen flow lamp. We provide VUV-absorption cross sections of the reported molecular ices. H_2S presents the highest absorption in the 120-160 nm range, while solid N_2 has the lowest VUV-absorption cross section, which is about three orders of magnitude lower than that of other species. Isotopic effects were studied for D_2O, $^{13}CO_2$, CD_3OD, and $^{15}N_2$. Our method allows fast and readily available VUV spectroscopy of ices without the need of using a synchrotron beamline. Photodesorption rates of pure ices, expressed in molecules per absorbed photon, can be derived from our data.

1 Introduction

Ice mantles in dense cloud interiors and cold circumstellar environments are composed mainly of H_2O and other species such as CO, CO_2, CH_4, CH_3OH, and NH_3 (Mumma & Charnley 2011 and ref. therein). Some species with no permanent or induced dipole moment such as O_2 and N_2, cannot be easily observed in the infrared, but are also expected to be present in the solid phase (e.g., Ehrenfreund & van Dishoeck 1998).

In the coldest regions where ice mantles form, thermally induced processes are inhibited. Therefore, irradiation processes by UV photons or cosmic rays may play an important role in the formation of new species in the ice and the desorption of ice species to the gas phase. In particular, cosmic rays penetrate deeper into the cloud interior than interstellar UV photons, generating a secondary

*cruzdiaz@strw.leidenuniv.nl

UV field by excitation of H_2 molecules. This secondary UV field interacts more intensively with the ice mantles than direct impact by cosmic rays (Cecchi-Pestellini & Aiello 1992, Chen et al. 2010). The vacuum ultraviolet (VUV) absorption spectrum as a function of photon wavelength is required to study and model these irradiation processes.

VUV-absorption cross sections have been only estimated for solid H_2O, NH_3, and CO_2 (Mason et al. 2006). Furthermore, all previous works have been performed using synchrotron monochromatic light as the VUV source. In the present work, we provide accurate measurements of the VUV-absorption cross sections of interstellar ice polar components (H_2O, CO, CH_3OH, NH_3, and H_2S; Cruz-Díaz et al. 2014a), apolar molecules (CO_2, CH_4, N_2, and O_2; Cruz-Díaz et al. 2014b), and four isotopologues of the previous species (D_2O, $^{13}CO_2$, CD_3OD, and $^{15}N_2$; Cruz-Díaz et al. 2014c). The use of a hydrogen VUV lamp in our experiments as the VUV source limits the spectroscopy to the emission range between 120 and 160 nm, but the measurements are easier to perform and can be made regularly in the laboratory, without the need of using synchrotron beam time.

In Sect. 2 the experimental protocol is described. Sect. 3 provides the VUV-absorption cross-section spectra for the different ice samples. The astrophysical implications are presented in Sect. 4.

2 Experimental protocol

The experiments were performed using the interstellar astrochemistry chamber (ISAC). This set-up and the standard experimental protocol were described in Muñoz Caro et al. (2010). ISAC mainly consists of an ultra-high-vacuum (UHV) chamber, with pressure typically in the range P = 3-4.0 $\times$ 10^{-11} mbar, where an ice analog made by deposition of a gas species onto a MgF_2 substrate at 8 K, achieved by means of a closed-cycle helium cryostat, can be UV-irradiated and/or heated. A schematic representation of ISAC is shown in Fig. 1.

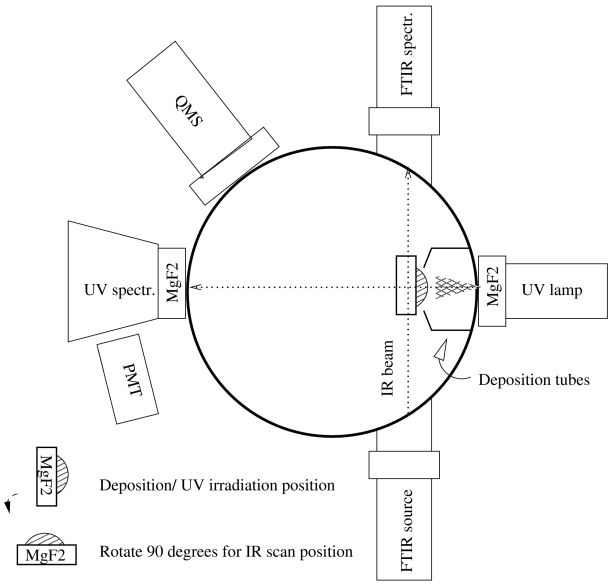

Figure 1: Scheme of the main chamber of ISAC. (Cruz-Díaz et al. 2014a; reproduced with permission from Astronomy & Astrophysics, ©ESO)

The deposited ice analog was photoprocessed with an F-type microwave-discharged hydrogen flow lamp (MDHL), from Opthos Instruments. The source has a VUV flux of $\approx 2 \times 10^{14}$ cm^{-2} s^{-1} at the sample position, measured by $CO_2 \rightarrow$ CO actinometry (Muñoz Caro et al. 2010). The Evenson

cavity of the lamp is refrigerated with air. The characterization of the MDHL spectrum has been studied before by Chen et al. (2010). The VUV-absorption spectrum is measured during the irradiation experiments with the use of a McPherson 0.2-meter focal length VUV monochromator (model 234/302) with a photomultiplier tube (PMT) detector equipped with a sodium salicylate window, optimized to operate from 100-500 nm (11.27-2.47 eV), with a resolution of 0.4 nm. The interface between the MDHL and the vacuum chamber is a MgF_2 window. The monochromator is located at the rear end of the chamber, separated by another MgF_2 window. This means that the measured background spectra are the result of the radiation that intersects two MgF_2 windows. Grating corrections were made for the VUV-absorption spectra in the range of 110-180 nm (11.27-6.88 eV). The mean photon energy was calculated for the spectrum corresponding to only one MgF_2 window intersecting the VUV-lamp emission, since that is the mean photon energy that the ice sample experiences. This one-window spectrum is displayed in Fig. 2.

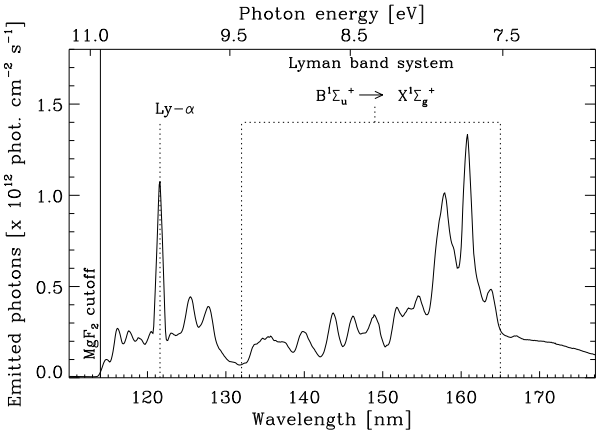

Figure 2: UV-photon flux as a function of wavelength of the MDHL in the 110 to 170 nm range estimated with the total photon flux calculated using actinometry. The spectrum corresponds to a measurement with one MgF_2 window intersecting the emitted VUV-light cone. This spectrum is the one experienced by the ice sample. The VUV emission is dominated by the Ly-α peak (121.6 nm) and the Lyman band system. (Cruz-Díaz et al. 2014a; reproduced with permission from Astronomy & Astrophysics, ©ESO)

It was observed that most of the energy emitted by the VUV lamp lies below 183 nm (6.77 eV) and the MgF_2 window cutoff occurs at 114 nm (10.87 eV). The mean photon energy in the 114-180 nm (10.87-6.88 eV) range is $E_{photon} = 8.6$ eV. The main emission bands are Ly-α at 121.6 nm (10.20 eV) and the molecular hydrogen bands centered on 157.8 nm (7.85 eV) and 160.8 nm (7.71 eV) for a hydrogen pressure of 0.4 mbar, see Fig.2.

The column density and the evolution of the ice sample was measured *in situ* by Fourier transform infrared (FTIR) in transmittance. The chemical components used were H_2O(liquid), triply distilled; CO(gas), Praxair 99.998%; CO_2(gas), Praxair 99.998%; CH_3OH(liquid), Panreac Química S. A. 99.9%; NH_3(gas), Praxair 99.999%; H_2S(gas), Praxair 99.8%; CH_4(gas), Praxair 99.999%; N_2(gas), Praxair 99.999%; O_2(gas), Praxair 99.8%; D_2O(liquid), Cambridge Isotope Laboratories, Inc (C.I.L.) 99.9%; CD_3OD(liquid), C.I.L. 99.8%; $^{13}CO_2$(gas), C.I.L. 99.0%; and $^{15}N_2$(gas), C.I.L. 98.0%.

3 Results

We recorded VUV-absorption spectra of pure ices. For each ice spectrum a series of three measurements was performed: i) the background spectrum, i.e., the emission spectrum of the VUV lamp, measured to monitor the intensity of the main emission bands, ii) the emission spectrum transmitted by the MgF_2 substrate window, measured to monitor its transmittance, and iii) the emission spectrum transmitted by the substrate window with the deposited ice on top. The VUV-absorption spectrum of the ice corresponds to the spectrum of the substrate with the ice after subtracting the bare MgF_2 substrate spectrum, i.e., iii) - ii).

The column density of the deposited ice obtained by FTIR was calculated according to the formula

$$N = \frac{1}{\mathcal{A}} \int_{band} \tau_\nu d\nu, \tag{1}$$

where N is the column density of the ice, τ_ν the optical depth of an infrared (IR) band, $d\nu$ the wavenumber differential, in cm^{-1}, and $\mathcal{A}$ is the band strength in cm $molecule^{-1}$. The integrated absorbance is equal to $0.43 \times \tau$, where τ is the integrated optical depth of the band.

Solid N_2, $^{15}N_2$ and O_2 do not display absorption features in the mid-infrared. Moreover, no IR band strength values were found in the literature for the D_2O and CD_3OD species. Therefore their column densities were measured using the expression

$$N = \frac{N_A \, \rho_i \, d_i}{m_i}, \tag{2}$$

where N_A is the Avogadro constant (6.022×10^{23} mol^{-1}), ρ_i is the density of the ice in g cm^{-3}, m_i is the molar mass of the species in g mol^{-1}, and d_i is the ice thickness in cm. The latter was estimated following the classical interfringe relation

$$d_i = \frac{1}{2 n_i \Delta\nu}, \tag{3}$$

where n_i is the refractive index of the ice at deposition temperature, and $\Delta\nu$ is the wavenumber difference between two adjacent maxima or minima of the fringes observed in the infrared spectrum of the ice. These interference fringes are due to multiple reflections of light within the sample.

The VUV spectrum and the column density of the ice were therefore monitored in a single experiment for the same ice sample. This improvement allowed us to estimate the VUV-absorption cross section of the ice more accurately. The VUV-absorption cross section was estimated according to the Beer-Lambert law,

$$I_t(\lambda) = I_0(\lambda) e^{-\sigma(\lambda) N} \tag{4}$$

$$\sigma(\lambda) = -\frac{1}{N} \ln\left(\frac{I_t(\lambda)}{I_0(\lambda)}\right) \tag{5}$$

where $I_t(\lambda)$ is the transmitted intensity for a given wavelength λ, $I_0(\lambda)$ the incident intensity, N is an average ice column density before and after irradiation in cm^{-2}, and σ is the cross section in cm^2.

3.1 VUV-absorption cross sections of interstellar polar ice analogs

3.1.1 Solid water

The VUV-absorption cross-section spectrum of H_2O ice is displayed in Fig.3. The band between 132-163 nm, centered on 142 nm (8.73 eV), is attributed to the $4a_1$:$\tilde{A}^1B_1 \leftarrow 1b_1$:$\tilde{X}^1A_1$ transition. The

VUV-absorption cross section reaches a value of $6.0^{+0.4}_{-0.4} \times 10^{-18}$ cm^{-2} at this peak. The portion of the band in the 120-132 nm range is attributed to the transition $\tilde{B}^1A_1 \leftarrow \tilde{X}^1A_1$, according to Lu et al. (2008). Gas-phase data from Mota et al. (2005) were adapted for comparison with our solid-phase data, see Fig. 3. The spectrum of water in the gas phase is redshifted with respect to the one of the solid phase and presents higher absorption cross-section values.

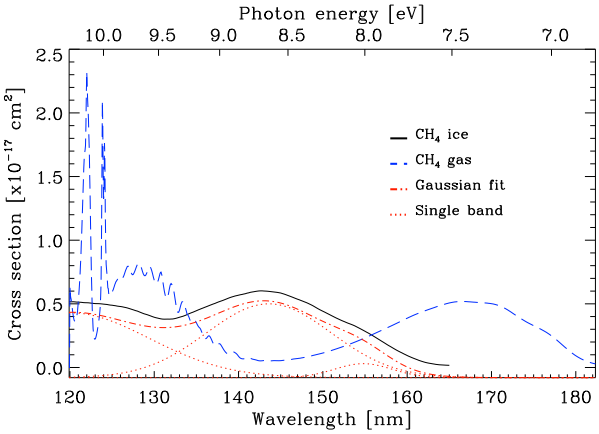

Figure 3: VUV-absorption cross section as a function of photon wavelength (bottom X-axis) and VUV-photon energy (top X-axis) of pure H_2O ice deposited at 8 K, black solid trace. The blue dashed trace is the VUV-absorption cross-section spectrum of gas phase H_2O taken from Mota et al. (2005). The fit, red dashed-dotted trace, is the sum of three Gaussians, dotted trace. It has been vertically offset for clarity. (Cruz-Díaz et al. 2014a; reproduced with permission from Astronomy & Astrophysics, ©ESO)

3.1.2 Solid carbon monoxide

Fig. 4 displays the CO fourth positive band system, attributed to the $A^1\Pi \leftarrow X^1\Sigma^+$ system. We were able to observe up to twelve bands corresponding to the vibrational structure of the same electronic transition, identified as (0,0) to (11,0). The (0,0), (1,0), and (2,0) bands present a Davydov splitting. We detected part of the transitions to the excited Rydberg states, $B^1\Sigma^+$, $C^1\Sigma^+$, and $E^1\Pi$ measured by Lu et al. (2005) as a broad band in the 116-121 nm (10.68-10.25 eV) region, despite the decreasing VUV-flux in this region.

3.1.3 Solid methanol

Fig. 5 shows the VUV-absorption cross section of CH_3OH as a function of wavelength and photon energy. Kuo et al. (2007) found three possible broad bands centered on 147 nm (8.43 eV), 118 nm (10.50 eV), and 106 nm (11.68 eV, beyond our spectral range). We observed the 147 nm peak (associated to the $2^1A'' \leftarrow X^1A'$ molecular transition) as well as part of the 118 nm band (corresponding to the $3^1A'' \leftarrow X^1A'$ molecular transition), but due to the decreasing VUV-flux below 120 nm it was not possible to confirm the exact position of this peak. Gas phase data from Nee et al. (1985) were used for comparison with our solid-phase spectrum, see Fig.5. CH_3OH gas has a vibrational peak profile throughtout the 120-173 nm range, which is absent in CH_3OH ice.

3.1.4 Solid ammonia

Fig. 6 displays the VUV-absorption cross section of NH_3 as a function of the photon wavelength and photon energy. It presents a continuum with two broad absorption bands between 120-151 nm (10.33-

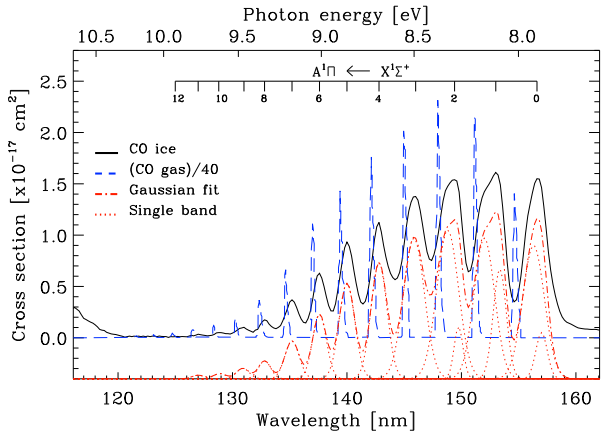

Figure 4: VUV-absorption cross section spectrum of pure CO ice deposited at 8 K, black solid trace. The spectrum of CO gas (divided by a factor of 40 to compare it with CO ice) has been adapted from Lee & Guest (1986). (Cruz-Díaz et al. 2014a; reproduced with permission from Astronomy & Astrophysics, ©ESO)

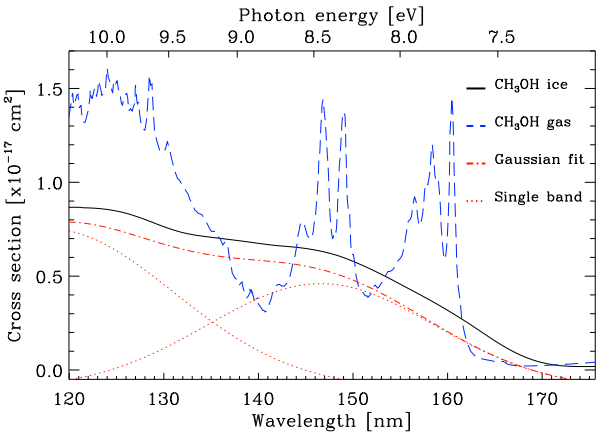

Figure 5: VUV-absorption cross section spectrum of pure CH_3OH ice deposited at 8 K, black solid trace. (Cruz-Díaz et al. 2014a; reproduced with permission from Astronomy & Astrophysics, ©ESO)

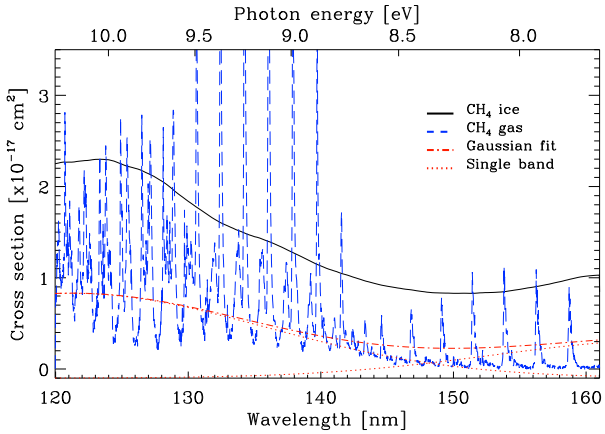

Figure 6: VUV-absorption cross section spectrum of pure NH_3 ice deposited at 8 K, black solid trace. The spectrum of gas phase NH_3 has been adapted from Cheng et al. (2006) and Wu et al. (2007). (Cruz-Díaz et al. 2014a; reproduced with permission from Astronomy & Astrophysics, ©ESO)

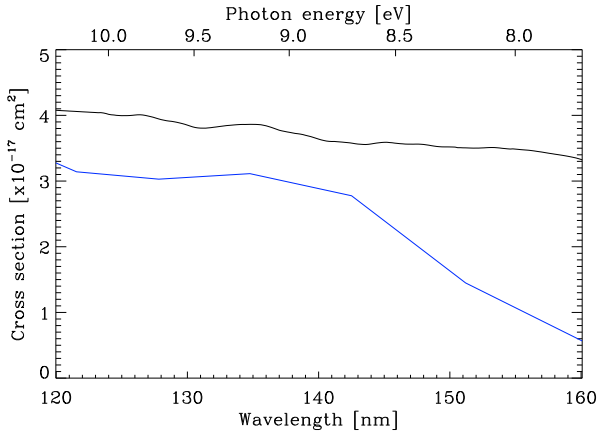

Figure 7: VUV-absorption cross-section spectrum of pure H_2S ice deposited at 8 K, black trace. The blue trace is the VUV-absorption cross-section spectrum of gas phase H_2S adapted from Feng et al. (1999) (Cruz-Díaz et al. 2014a; reproduced with permission from Astronomy & Astrophysics, ©ESO)

8.21 eV) and 151-163 nm (8.21-7.60 eV) in this wavelength region, without narrow bands associated to vibrational structure. We observed only a portion of the feature in the 163-180 nm (7.60-6.88 eV) spectral range because of the low VUV-flux of the MDHL in that range. This band is associated to the $\tilde{A}^1A_2$" $\leftarrow \tilde{X}^1A_1$ molecular transition. As for CH_3OH, the absorption spectrum of gaseous ammonia also presents vibrational structure.

3.1.5 Solid hydrogen sulfide

Fig. 7 shows the VUV-absorption cross section of H_2S as a function of the wavelength and photon energy. Owing to the high VUV-absorption of solid H_2S, very thin ice samples were deposited to obtain a proper VUV-spectrum. Solid H_2S has an almost constant UV-absorption cross section in the studied range, while gaseous H_2S presents a decrease at wavelengths longer than $\sim$ 143 nm. The $^1B_1 \leftarrow {}^1A_1$ molecular transition was identified at 139.1 nm (8.91 eV) by Price & Simpson (1938) and confirmed by Gallo & Innes (1975).

3.2 VUV-absorption cross section of interstellar apolar ice analogs

3.2.1 Solid carbon dioxide

The VUV-absorption cross section of CO_2 as a function of the wavelength and photon energy is shown in Fig. 8. Two broad bands in the 120-133 nm (10.33-9.32 eV) and 133-163 nm (9.32-7.60 eV) regions are observed in our spectrum. A faint vibrational structure is detected in the 120-133 nm band. Photoprocessing of the CO_2 ice efficiently leads to the formation of CO by photodissociation of CO_2 molecules. After 9 minutes, corresponding to the collection time of a spectrum, CO is present with a column density that is 22 % of the deposited CO_2 column density, which is enough to appear in the VUV-spectrum of CO_2 ice in the 133-167 nm wavelength range. Because of the interaction of CO molecules with the CO_2 ice matrix, the CO features are shifted to shorter wavelengths than those of pure CO ice.

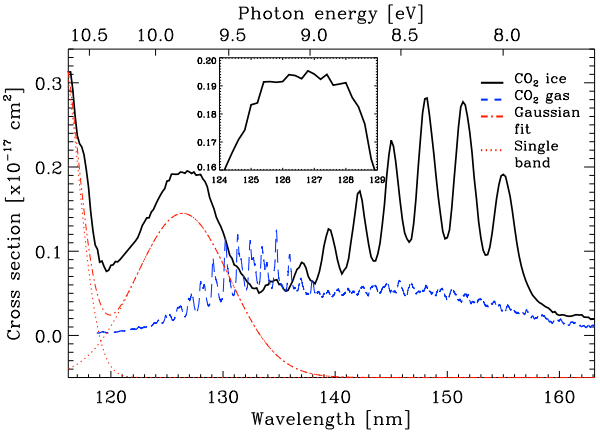

Figure 8: VUV-absorption cross-section of CO_2 ice deposited at 8 K, black solid trace. The spectrum of gas phase CO_2 has been adapted from Yoshino et al. (1996). The inset figure is a CO_2 VUV-absorption cross-section close-up in the 124-129 nm range. (Cruz-Díaz et al. 2014b; reproduced with permission from Astronomy & Astrophysics, ©ESO)

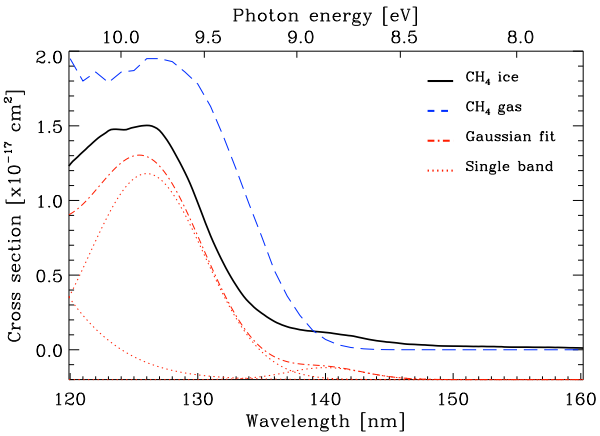

Figure 9: VUV-absorption cross-section spectrum of CH_4 ice deposited at 8 K, black solid trace. The spectrum of gas phase CH_4 has been adapted from Lee et al. (2001).

3.2.2 Solid methane

Fig. 9 shows the VUV-absorption cross section of CH_4 as a function of the wavelength and photon energy. A broad absorption band extending to 137 nm (9.05 eV) and centered on 124 nm (10.0 eV) is

observed. This feature is attributed to the $1t_2$-3s (D_{2d}) Rydberg transition. We also detected a small bump near 140 nm (8.85 eV), which may be produced by a photoproduct (not detected by infrared spectroscopy).

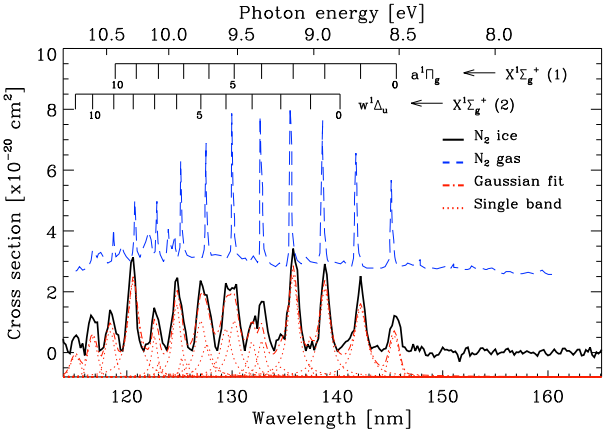

Figure 10: VUV-absorption cross-section spectrum of N_2 ice deposited at 8 K, black solid trace. Gaseous spectrum adapted from Mason et al. (2006). (Cruz-Díaz et al. 2014b; reproduced with permission from Astronomy & Astrophysics, ©ESO)

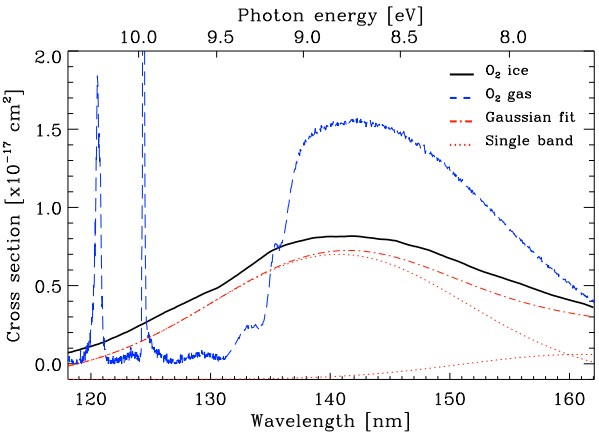

Figure 11: VUV-absorption cross-section spectrum of O_2 ice deposited at 8 K, black solid trace. (Cruz-Díaz et al. 2014b; reproduced with permission from Astronomy & Astrophysics, ©ESO)

3.2.3 Solid nitrogen

Owing to its very low VUV-absorption cross section (several orders of magnitude lower than the rest of the studied ices), a deposition of 2.36 μm, nearly 4.7 $\times$ 10^{18} molecules cm^{-2}, for N_2 ice was required to detect the absorption features. The VUV-absorption cross section as a function of wavelength and photon energy is shown in Fig. 10. It presents two overlapping band systems corresponding to the vibrational structure of two different electronic transitions (attributed to $a^1\Pi_g \leftarrow X^1\Sigma_g^+$ and $w^1\Delta_u \leftarrow X^1\Sigma_g^+$) in the 114-147 nm (10.87-8.43 eV) region.

3.2.4 Solid oxygen

The VUV-absorption cross section as a function of wavelength and photon energy is shown in Fig. 11. Solid O_2 presents a broad band centered on 141 nm (8.79 eV) in the 118-162 nm (10.50-7.65 eV) region (attributed to the $\tilde{B}^3\Sigma_u^- \leftarrow X^3\Sigma_g^-$ transition, named Schumann-Runge band). Gas-phase data from Lu et al. (2010) were used for comparison with our solid phase data, see Fig. 11. The gas-phase spectrum presents two discrete transitions at shorter wavelengths, not observed in the solid phase.

3.3 VUV-absorption cross section of heavy isotopologues

We also registered the VUV-absorption cross-section spectra of four heavy isotopologues of the previous species, to study the influence of isotopic substitution. As it is shown in Figures 12, 13, 14, and 15, this only leads to small blueshifts in the peak positions, with no major effects.

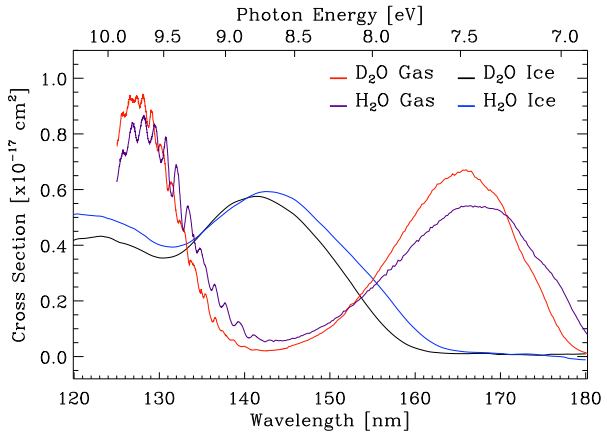

Figure 12: VUV-absorption cross-section spectrum of solid and gaseous H_2O, and D_2O. Spectra of gas phase D_2O and H_2O adapted from Cheng et al. (2004) and Chung et al. (2001), respectively. (Adapted from Cruz-Díaz et al. 2014c).

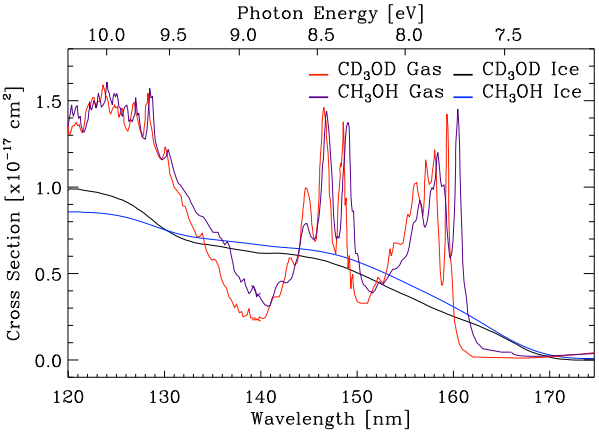

Figure 13: VUV-absorption cross-section spectrum of solid and gaseous CD_3OD. The spectra of the gas-phase molecules have been adapted from Cheng et al. (2002). (Adapted from Cruz-Díaz et al. 2014c).

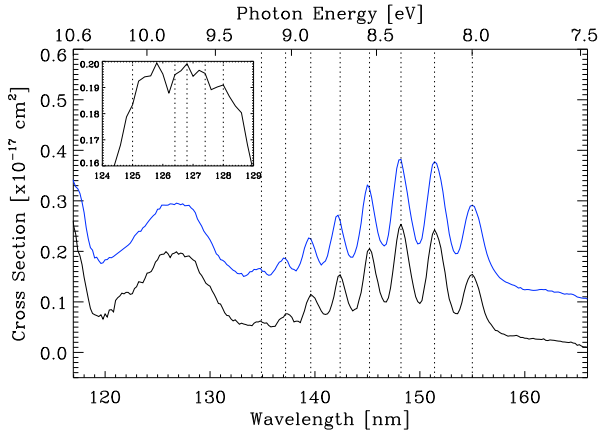

Figure 14: VUV-absorption cross-section spectrum of solid $^{13}CO_2$ (black trace) and CO_2 (blue trace) offset for clarity. The faint vibrational structure (inlet) may be slightly different compared to the main isotopologue case. (Adapted from Cruz-Díaz et al. 2014c).

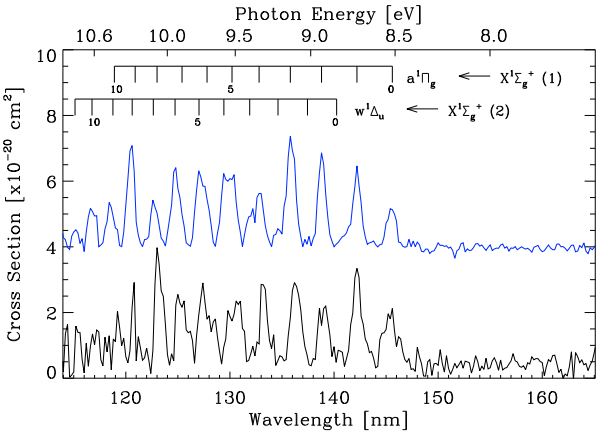

Figure 15: VUV-absorption cross-section spectrum of solid $^{15}N_2$ (black trace) and N_2 (blue trace) offset for clarity. (Adapted from Cruz-Díaz et al. 2014c).

4 Astrophysical implications

The most straightforward application of these results is the study of the photodesorption processes that may play an important role in dense cloud interiors. There is a clear correspondence between the photodesorption rates of CO ice measured at different photon energies (Fayolle et al. 2011) and the VUV-absorption spectrum of CO ice (this work) for the same photon energies. This indicates that photodesorption of some ice species like CO and N_2 is mainly driven by a desorption induced by electronic transition (DIET) process (Fayolle et al. 2011; 2013).

In addition, the photodesorption rate per absorbed photon in the $[\lambda_i,\lambda_f]$ wavelength range, $R_{\rm ph-des}^{\rm abs}$, can differ significantly from the photodesorption rate per incident photon, $R_{\rm ph-des}^{\rm inc}$. It can be estimated

as follows:

$$R^{\rm abs}_{\rm ph-des} = \frac{\Delta N}{I_{abs}} \quad and \quad R^{\rm inc}_{\rm ph-des} = \frac{\Delta N}{I_0}$$

$$R^{\rm abs}_{\rm ph-des} = \frac{I_0}{I_{abs}} R^{\rm inc}_{\rm ph-des}, \tag{6}$$

where

$$I_{abs} = \sum_{\lambda_i}^{\lambda_f} I_0(\lambda) - I(\lambda) = \sum_{\lambda_i}^{\lambda_f} I_0(\lambda)(1 - e^{-\sigma(\lambda)N}),$$

and ΔN is the column density decrease for a given irradiation time in molecules cm^{-2} s^{-1}, I_0 is the total photon flux emitted, I_{abs} is the total photon flux absorbed by the ice, $I_0(\lambda)$ is the photon flux emitted at wavelength λ, $\sigma(\lambda)$ is the VUV absorption cross section at the same wavelength, and N is the column density of the ice sample. Table 1 presents different values of $R^{\rm inc}_{\rm ph-des}$ and $R^{\rm abs}_{\rm ph-des}$ for several monochromatic irradiations (Fayolle et al. 2011), and for a continuum source (this work) with a mean photon energy of 8.6 eV. The main conclusion is that one only photon can induce photodesorption of more than one molecule.

Table 1: VUV-absorption cross sections for different irradiation energies.

Irrad. energy eV	σ cm^2	$R^{\rm inc}_{\rm ph-des}$ molec./photon$_{inc}$	$R^{\rm abs}_{\rm ph-des}$ molec./photon$_{abs}$
10.2	1.1×10^{-19}	$6.9 \pm 2.4 \times 10^{-3}$	12.5 ± 4.4
9.2	2.8×10^{-18}	$1.3 \pm 0.91 \times 10^{-2}$	0.9 ± 0.6
† 8.2	9.3×10^{-18}	5×10^{-2}	1.1
8.6	4.7×10^{-18}	$5.1 \pm 0.2 \times 10^{-2}$	2.5 ± 0.1

†Peak yield value at $\sim$ 8.2 eV, see Fayolle et al. (2011).

Acknowledgements

This research was financed by the Spanish MINECO (projects AYA2011-29375 and CONSOLIDER grant CSD2009-00038). R. M. D. and G.A.C.D. benefited from a FPI grant from Spanish MINECO.

References

Brith, M., & Schnepp, O. 1965, Molecular Phys., 9, 473
Cecchi-Pestellini, & Aiello, S. 1992, MNRAS, 258, 125
Chen, Y.-J., Chu, C.-C, Lin, Y.-C, et al. 2010, Advances in Geosciences, 25, 259
Cheng B.-M., Bahou M., Chen W.C., Yui C.H., Lee Y.-P., Lee, L.C., 2002, Journal of Chem. Phys., 117, 1633.
Cheng, B.-M., Lu, H.-C., Chen, H.-K., et al. 2006, ApJ, 647, 1535
Chung C.-Y., Chew E.P., Cheng B.-M., Bahoub M., Lee Y.-P., 2001, Nucl. Instr. Meth. Phys. Res. A, 467, 1572.
Cruz-Díaz, G.A., Muñoz Caro, G.M., Chen, Y.-J., & Yih, T.S., 2014a, A&A, 562, A119
Cruz-Díaz, G.A., Muñoz Caro, G.M., Chen, Y.-J., & Yih, T.S., 2014b, A&A, 562, A120
Cruz-Díaz, G.A., Muñoz Caro, G.M., & Chen, Y.-J., 2014c, MNRAS, 439, 2370
d'Hendecourt, L. B., Allamandola, L. J., & Greenberg, J. M. 1985. A&A, 152, 130
d'Hendecourt, L. B., Allamandola, L. J., Grim, R. J. A., & Greenberg, J. M. 1986. A&A, 158, 119

Ehrenfreund, P., & van Dishoeck, E. F. 1998, Advances in Space Research, 21, 15
Fayolle, E. C., Bertin, M., Romanzin, C., et al. 2011, ApJ Letters, 739, L36
Fayolle, E. C., Bertin, M., Romanzin, C., et al. 2013, A&A, 556, A122
Feng, R., Cooper, G., & Brion, C. E. 1999, Chem. Phys., 244, 127
Fillion, J.-H., Bertin, M., Lekic, A., et al. 2012, EAS Publications Series, 58, 307
Gallo, A. R., & Innes, K.K. 1975, J. Mol. Spectrosc., 54, 472
Gerakines, P. A., Schutte, W. A., Greenberg, J. M. & van Dishoeck, E. F. 1995. A&A, 296, 810
Gerakines, P. A., Schutte, W. A. & Ehrenfreund, P., 1996, A&A, 312, 289
Kuo, Y.-P., Lu, H.-C., Wu, Y.-J., Cheng, B.-M., & Ogilvie, J. F. 2007, Chem. Phys. Lett., 447, 168
Lee, L. C., & Guest, J. A. 1981, J. Phys. B: At. Mol. Phys., 14, 3415
Lee, A. Y. T., Yung, Y. L., Cheng, B.-M., et al., 2001, ApJ Lett., 551, L93
Lu, H.-C., Chen, H.-K., Cheng, B.-M., Kuo, Y.-P., & Ogilvie, J. F. 2005, J. Phys. B: At. Mol. Opt. Phys., 38, 3693
Lu, H.-C., Chen, H.-K., Cheng, B.-M., & Ogilvie, J. F. 2008, SAA, 71, 1485
Lu, H. -C., Chen, H. -K., Chen, H. -F., Cheng, B. -M. & Ogilvie, J. F., 2010, A&A, 520, A19
Mason, N. J., Dawes, A., Holton, P. D., et al. 2006, Faraday Discussions, 133, 311
Mota, R., Parafita, R., Giuliani, A., et al. 2005, Chem. Phys. Lett., 416, 152
Mumma, M. J., & Charnley, S. B. 2011, Annu. Rev. Astro. Astrophys., 49, 471
Muñoz Caro, G.M., Jiménez-Escobar, A., Martín-Gago, J.A., et al. 2010, A&A, 522, A108
Nee, J. B., Suto, M., & Lee, L. C. 1985, Chemical Physics, 98, 147
Price, W. C., & Simpson, D. M. 1938, Proc. Roy. Soc. (Lond.), A165, 272
Sandford, S. A. 1996. Astronomical Society of the Pacific Conference Series, 97, 29
Schutte, W. A. 1996. Molecules in Astrophysics: Probes and Processes, IAU symposium 178, 1
Öberg, K. I., Garrod, R. T., van Dishoeck, E. F., & Linnartz, H. 2009a. A&A, 504, 891
Öberg, K. I., Linnartz, H., Visser, R., & van Dishoeck, E. F. 2009b. ApJ, 693, 1209
Yoshino, K., Esmond, J. R., Sun, Y., et al., 1996, J. Quant. Spectrosc. Radiat. Transfer, 55, 53
Wu, Y.-J., Lu, H.-C., Chen, H.-K., & Cheng, B.-M. 2007, J. Chem. Phys., 127, 154311